Soft Matter

Active binary mixtures of fast and slow hard spheres

SCHOLARONE™
Manuscripts

Active binary mixtures of fast and slow hard spheres[†]

Thomas Kolb[ab] and Daphne Klotsa[*b]

We computationally studied the phase behavior and dynamics of binary mixtures of active particles, where each 'species' had distinct activities leading to distinct velocities, fast and slow. We obtained phase diagrams demonstrating motility-induced phase separation (MIPS) upon varying the activity and concentration of each species, and extended current kinetic theory of active/passive mixtures to active/active mixtures. We discovered two regimes of behavior quantified through the participation of each species in the dense phase compared to their monodisperse counterparts. In regime I (active/passive and active/weakly-active), we found that the dense phase was segregated by particle type into domains of fast and slow particles. Moreover, fast particles were suppressed from entering the dense phase while slow particles were enhanced entering the dense phase, compared to monodisperse systems of all-fast or all-slow particles. These effects decayed asymptotically as the activity of the slow species increased, approaching the activity of the fast species until they were negligible (regime II). In regime II, the dense phase was homogeneously mixed and each species participated in the dense phase as if it were it a monodisperse system; each species participated in the dense phase as if it were not mixed at all. Finally, we showed that a weighted average of constituent particle activities, which we term the net activity, defines a binodal for the MIPS transition in active/active binary mixtures. We examined the critical point of the transition and found a critical exponent ($\beta = 3/4$) that is distinct from known monodisperse active-matter systems and equilibrium systems.

1 Introduction

From schools of sardines to flocks of starling, the complex, collective behavior found in natural swarms has spurred an interest in active-matter systems, where constituents locally convert energy into motion. At high constituent particle densities, such systems can be viewed as "living" materials with the ability to do work and adapt to stimuli, heal themselves, *etc.* similar to *e.g.* biological tissue. The remarkable properties of active matter (self-healing, responsiveness, adaptation, *etc.*) can be leveraged in experimental setups to complete tasks and do work on the microscopic scale, *e.g.* bacteria can be used to turn a microscopic gear[1].

Simple models have been developed to capture the emergent behavior of active matter, including the Vicsek model[2] inspired by bird flocks, run-and-tumble[3–5] by bacterial swarms, and the active Brownian particle (ABP)[5,6] by self-propelled colloids. These models have demonstrated a variety of unusual nonequilibrium states, such as robust flocking bands[7], upstream swimming of bacteria[8] and a negative surface tension for active droplets[9,10] respectively. Since the inception of the field, many equilibrium mappings have been posited using a variety of effective thermodynamic parameters, including temperature[11–13], free energy[14,15], and pair-wise potentials[16–19]. These approaches have met varying degrees of success and function well for specific cases. For example, by quantifying the violation of a Maxwell construction on the pressure developed by Solon et al.[20], the phase diagram for monodisperse ABPs can be reproduced exactly[21].

The standard ABP model consists of a monodisperse system of active hard spheres confined to a plane. In the absence of any attractive potential between particles, and at sufficient activity, the system phase separates (either gas/liquid or gas/solid), in a process known as motility-induced phase separation (MIPS), see ref. 5 for a review and references therein. The predicted MIPS was recapitulated in experiment with light-activated carbon-coated Janus particles[22] and has since been adapted to a variety of experimental set-ups which depend on either light, magnetic/electric fields, or acoustics to induce phoresis, see review[23]. The ABP model has also been implemented with additional complexities *e.g.* confinement[19,24–26], anisotropy in particle shape[27],

[a] *Department of Chemistry, University of North Carolina at Chapel Hill, USA*

[b] *Department of Applied Physical Sciences, University of North Carolina at Chapel Hill, USA*

particle interactions[28] and size polydispersity[24,29,30] leading to the discovery of new emergent phenomena, such as particle sorting and segregation.

Recent work has shown that mixtures of active and passive Brownian particles also display MIPS, similar to a monodisperse active system[31,32]. Under certain parameters, for example, steady states emerge wherein particles partially segregate into active and passive domains[31,32]. Mixtures provide an additional degree of control for performing specific functions. For example, doping a monodisperse Brownian system with active particles can help anneal crystals and rapidly relax jammed states[33,34].

However, active living systems interact not only with passive Brownian particles and obstacles but also with other active species. In nature we encounter a wealth of active/active systems ranging in scale from the microscopic (*e.g.* mixtures of bacteria with different motility mechanisms[35] or speeds[36] and microorganism swarms[37]) to the macroscopic (*e.g.* sheep herded by sheepdogs[38], or in the emergent flocking structure of pigeons[39]). From a materials applications standpoint, it is reasonable to expect that mixtures of particles with various activities would provide more control and allow the exploration of novel assembling and swarming states, resulting in additional functionality.

From a theoretical point of view, mixtures of active particles are extremely relevant in trying to define effective thermodynamic quantities in active matter in general. Consider the analogy to equilibrium systems, described in ref. 12: a non-active mixture of two types of particles at different initial temperatures, hot and cold. As the system thermally equilibrates over time, information is conveyed between particles (the hot and cold particles' kinetic energies), and the system reaches thermodynamic equilibrium, governed by the initial number and temperature of each type of particle. For a monodisperse active system of ABPs, it is well-known that the particle activity sets the emergent phase behavior of the system. But, what (if any) quantity equilibrates in a mixture of active particles distinct in their activity? Thus to further understand the existence of effective thermodynamic quantities, a binary mixture of two distinctly active particles provides an ideal context.

Simple models such as the ABP, which has been used to aid much of the theory developed in active-matter systems, can be used to study active/active mixtures too. While there is a lot of work on monodisperse ABPs and more recently on mixtures of active and passive particles, the ABP model has not yet been applied to mixtures of active particles with distinct, non-zero, activity. (We note that other models have been used to examine mixtures of two active constituents e.g. oppositely spinning active rotors[40,41], particles propelled by distinct colored noise[42], polymers and colloids equilibrating in distinct heat baths[43–45] and monodisperse ABPs and moving obstacles[46].)

In this paper, we computationally studied binary active mixtures of 'fast' and 'slow' particles, using the ABP model. We first obtained phase diagrams for active/active mixtures relating area fraction and activity, and extended the kinetic theory of Stenhammar *et al.*[31] to include two active species. We discovered two regimes of behavior quantified through the participation of each species (fast and slow) in the dense phase compared to a monodisperse system of each type. In regime I (active/passive and active/weakly-active), we found that the dense phase was strongly segregated by particle type; the edge comprised primarily of fast particles, with domains of slow particles populating the cluster interior. Additionally, in the first regime, fast particles were suppressed from entering the dense phase while slow particles were enhanced entering the dense phase, compared to a monodisperse system of all-fast or all-slow particles. These effects decayed asymptotically until they were negligible in regime II. In regime II, the dense phase was homogeneously mixed and each species participated in the dense phase as it would if it were not mixed at all. Finally, we defined the net activity, which is an average of each constituent particle's activity weighted by its area fraction. We demonstrated the utility of the net activity in defining the binodal envelope, and investigated a critical exponent of this first-order phase transition via a reduced inverse net activity, and found a critical exponent ($\beta = 3/4$) distinct from critical exponents in monodisperse active-matter[47] systems or equilibrium systems.

The structure of the paper is as follows. In section 2 we outline the theoretical and computational methods, and simulation details for the active systems studied here. In section 3, we discuss background, and specifically previous studies of monodisperse active and mixtures of active/passive systems. We describe our results in section 4, and end with conclusions and outlook in section 5.

2 Methods

Our system approximates the physics of active colloids confined to a plane. We used N spheres, each with a body axis that indicates a particle's direction of self-propulsion (restricted to be in-plane). Particles translate and rotate according to the overdamped Langevin equations of motion for translation and rotation:

$$\gamma \dot{\vec{r}}_i = F_{WCA}(\vec{r}_i) + F_{act}\hat{p}_i + \gamma\sqrt{2D_t}\Lambda_i^t \tag{1}$$

$$\dot{\theta}_i = \sqrt{2D_r}\Lambda_i^r \quad , \tag{2}$$

where r_i is the position of particle i, $\hat{p}_i = (\cos\theta_i, \sin\theta_i)$ gives its orientation in the xy-plane, F_{WCA} is the conservative force due to pairwise interactions, F_{act} is a particle's active force, D_t and D_r are the translational and rotational diffusion constants, and γ is the drag coefficient. The random force incorporates unit variance Gaussian white noise, implemented through Λ^t for translation and Λ^r for rotation such that $\langle\Lambda_i\rangle = 0$ and $\langle\Lambda_i(t)\Lambda_j(t')\rangle = \delta_{ij}\delta(t-t')$. In overdamped systems (low Reynolds number), the Stokes-Einstein equation gives $D_t = \frac{k_BT}{3\pi\eta\sigma} = \frac{k_BT}{\gamma}$ and $D_r = \frac{3D_t}{\sigma^2}$, where σ is the particle diameter, η the dynamic viscosity, and k_BT the thermal energy. We used σ as the non-dimensional unit of distance.

Activity was quantified through the Péclet number:

$$Pe = \frac{3v_0\tau_r}{\sigma}, \tag{3}$$

where (v_0) is the intrinsic swim speed, *i.e.* the speed of an active particle under the action of the active force F_{act} (in the absence of collisions), and τ_r is the reorientation time, given by $\tau_r = D_r^{-1}$.

Note that, while in the present model reorientation is set according to the system temperature, our results need not be restricted to particles of a specific size at a set temperature. Often, the reorientation of active particles stems from other sources such as hydrodynamic interactions [48] or chemical gradients [49,50]. Indeed, our results are applicable when τ_r is not thermal in nature, as the Péclet number defined in equation 3 encodes the persistence length which is given by $l_p = v_0 \tau_r$. The persistence length quantifies how far an active particle travels maintaining its direction before it undergoes a rotation event (in this case, due to continuous thermal rotation).

In simulations, we varied the active force, $F_{act} = v_0 \gamma \hat{p}$ via the intrinsic swim speed. This was intentionally distinct from other works, where activity was modulated through the diffusion constant by varying the system temperature [31,32,51]. While both temperature-variant and velocity-variant models encode the same persistence length for a given activity, an important distinction arises when examining mixtures of active particles. In simulations of binary active mixtures (say A and B, with activities $Pe_B > Pe_A$) using a temperature-variant model, the difference between distinct particle types arises through the reorientation timescale, where the more active particle will undergo reorientation less often ($\tau_r^B > \tau_r^A$) and therefore have a greater persistence length ($l_p^B > l_p^A$). However, particles will move with the same velocity and thereby experience an identical active force ($F_{act}^B = F_{act}^A$). In contrast, in our velocity-variant model, a more active particle will experience a greater active force ($F_{act}^B > F_{act}^A$), causing it to swim faster ($v_0^B > v_0^A$) while undergoing reorientation events with the same frequency as the slower particle type ($\tau_r^B = \tau_r^A$), still resulting in a greater persistence length ($l_p^B > l_p^A$). In examinations of MIPS, it has been shown that particle rotation controls the rate of desorption from the dense phase, such that the faster the particle rotation the larger the rate of desorption from the dense phase [52,53]. As a temperature-variant model directly changes the rotational diffusion between particle types, it would also bias the composition of the cluster edges to have more of the slowly-rotating, fast species. To summarize, the velocity-variant model is useful for systems where reorientation stems from the same effect but particles swim at different speeds whereas the temperature-variant model is applicable to systems where constituents move at the same speed but reorient on different timescales. In this study, we chose to use the velocity-variant model so as to study particles with distinct swim speeds.

All particles, regardless of type, experience excluded volume interactions via a Weeks-Chandler-Andersen (WCA) potential,

$$U(r_{i,j}) = \begin{cases} 4\varepsilon[(\frac{\sigma}{r_{i,j}})^{12} - (\frac{\sigma}{r_{i,j}})^6] + \varepsilon & 0 \leq r_{i,j} \leq \sqrt[6]{2}\sigma \\ 0 & r_{i,j} > \sqrt[6]{2}\sigma, \end{cases}$$ (4)

with corresponding force,

$$F_{WCA}(r_{i,j} \leq r_{cut}) = 24\varepsilon \left(2\frac{\sigma^{12}}{r^{13}} - \frac{\sigma^6}{r^7} \right)$$ (5)

where r_{ij} is the interparticle distance between the ith and j^{th} particles (with potential cutoff at $r_{cut} = \sqrt[6]{2}\sigma$). To nondimen-

sionalize our system we set $\sigma = 1$ as the particle diameter, and $\varepsilon = k_B T(\alpha + 10)$ as the potential well depth, where α is an activity-dependent coefficient ($\alpha \sim F_{act}\sigma$) implemented to maintain a constant, hard sphere, particle diameter. For passive particles, the repulsive well depth reduces to $\varepsilon = 10k_B T$. To maintain a constant particle diameter we consider the greatest force present at a given set of parameters; in a Brownian system this is the thermal force. As first acknowledged by Stenhammar et al. [51], this is not the case in active systems where the active force typically exceeds the thermal force. If we used the thermal force to set the repulsive strength, particles would, on average, experience a large degree of overlap (reducing the diameter by 25% of the intended value). To determine the coefficient (α) and thus interaction well depth ε that corresponds to hard spheres we performed simulations on monodisperse active systems, as well as binary active/passive, and active/active ones, with $\varepsilon = k_B T$ at total area fraction, $\phi = 0.6$. We then extracted all the particle diameters that occur in the simulations (δ) and plotted a histogram for $\delta \leq r_{cut}$.

For a hard sphere system, we expect a narrow distribution of measured particle diameters where the peak (mode) of the histogram, we shall call it the effective diameter, is equal to the intended (hard-sphere) diameter ($\sigma_{eff} = \sigma = 1$). Measured particle diameters less than the intended diameter ($\delta < 1$) indicate that there are instances when the forces are larger than accounted for by the repulsive pairwise potential and thus particles become slightly "soft". Indeed, this commonly occurs when the repulsive depth is set by the thermal force ($\varepsilon = k_B T$). The histogram for these data exhibited values far lower than the intended particle diameter (fig. 1b, $\delta < 1$).

To prevent this, we extracted the mode of the distribution (σ_{eff}) at several activities and particle fractions and substituted back into equation 5 as r, to obtain the most common force experienced by the particles. We then used that force on the left-hand side of equation 5, with $\sigma = r = 1$ (for hard spheres) and solved for the interaction well depth required to prevent significant particle overlap (ε_{req}). For monodisperse systems, plotting the effective diameter as a function of activity produced an interaction well depth similar to that predicted by ref. 51: $\varepsilon_{req} = 4F_{act}\sigma/24$ (fig. 1c, black diamonds), where an increasing active force corresponds to a smaller effective diameter and therefore a larger required repulsive force (to correct for emergent particle softness).

In a binary mixture three potentials must be considered for interactions between: fast-fast, fast-slow, and slow-slow particles. As such, we broke down our diameter analysis by interaction type. Our data showed that all interactions for a given simulation predict the same interaction well depth (ε_{req}, fig. 1c inset). Additionally, we found that the magnitude of the interaction well depth should be weighted according to the particle fraction of each type (fig. 1c inset). This gave the following relationship for the interaction well depth that was used in our studies,

$$\varepsilon_{req.} = \left(\frac{4(F_s x_s + F_f x_f)}{24} + 10 \right) k_B T$$ (6)

As the interaction well depth incorporates the fraction of each species, this implementation correctly reduces to $\alpha = 4F_{act}\sigma/24$ in the monodisperse case, (fig. 1c inset $x_f = 0, 1$).
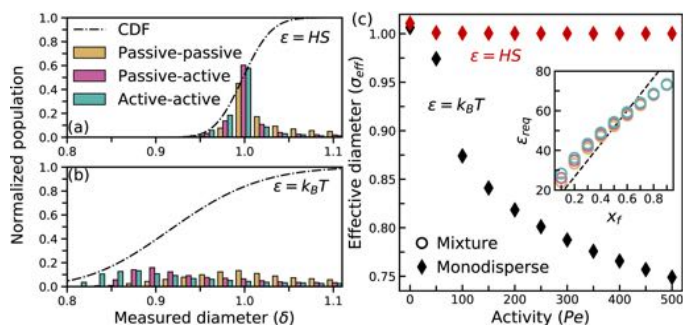
Fig. 1 Comparison of particle activity and interparticle distance for particle pairs within the WCA interaction cutoff ($0 \leq r \leq r_{cut}$). (Left) Histograms of the measured diameters as they occur in our simulations, separating interactions between passive-passive, passive-active and active-active, as well as showing the cumulative distribution function (CDF) overlaid. CDF displays the probability of a particle having diameter $\leq x$. Data are computed for an active/passive simulation with $x_f = 0.1$ and $Pe_f = 500$. (a) Histogram and CDF for simulations performed using ε from equation 6 demonstrates that no particles have measured diameter $\delta \leq 0.95$ while 50% of particles have measured diameters $0.95 < \delta \leq 1.00$. (b) Histogram and CDF for simulations using $\varepsilon = k_B T$ where all types of interaction data deviate well below the intended diameter. (c) Plot of the effective diameter measured in simulation as a function of particle activity. Simulation data for monodisperse simulations with well depth $\varepsilon = k_B T$ (black) shows drastic particle overlap as activity is increased. Data for systems simulated with interaction potential according to equation 6 (red), maintains a constant mode center-to-center distance that is equal to the intended diameter ($= 1$ for hard spheres). Inset shows predicted ε both from equation 6 (dashed line) and computed from emergent simulation data with respect to system composition. Required well depth is computed for passive-passive (gold), passive-active (pink), and active-active (teal) interactions.

We consider this to be a hard-sphere model in that it satisfies the following two requirements: (1) the most commonly occurring particle diameter for each particle type is the intended hard sphere diameter (fig 1c, red diamonds) and (2) the largest deviation from the intended diameter is at most 5% (fig 1a). Given this definition, we found that our implementation for the repulsive force can consistently be considered a hard-sphere one, irrespective of activity or particle fraction (see fig. 1a, c, red diamonds).

Implementing the interparticle potential according to equation 6 affects the maximum timestep permitted for a given simulation ($dt_{max} = 1 \times 10^{-5} \cdot (\sigma^2 \gamma / \varepsilon)$). Since we chose to vary the swim velocity in our model, we also need to vary the potential well depth and the timestep. Therefore, we present our results using the temperature-dependent (and invariant) timescale for the persistence of motion, τ_r. We also performed convergence studies on our model to determine the necessary ratio of $l_p : l_{box}$ to avoid finite size effects at the densities and activities used in this study (see ESI, fig. S1).

2.1 Simulation Parameters and definitions

Simulations were performed using the GPU-enabled Molecular Dynamics package available in HOOMD-blue[54,55]. We initialized particles randomly (allowing a slight particle overlap, $\delta = 0.70$) and then equilibrated the system via Brownian dynamics for $30\tau_r$. After equilibration, simulations were run for $300\tau_r$. Total system

area fraction was constant at $\phi = 0.6$. At this area fraction, systems were above the minimum density required to display phase separation ($\phi \approx 0.45$) and at the estimated critical area fraction for monodisperse MIPS ($\phi \approx 0.6$)[15,47,56].

The onset of MIPS was initially analyzed by a cluster algorithm[57] with a cutoff that was calibrated on simulations of monodisperse active particles ($Pe = 30$) below the activity required for phase separation at the system density used in this study ($Pe_{MIPS} \approx 45$ for $\phi = 0.6$). At this activity ($Pe = 30$), the system does not undergo MIPS, however, small, short-lived clusters will regularly form and fall apart. Thus it gives us the largest signal for transient clusters that are not truly phase separated both in terms of size and lifetime. For simulations proximal to the binodal, our algorithm was often insufficient in delineating which systems were phase-separated due to the large fluctuations in the number and size of transient clusters. So, in addition to the algorithm, we examined the phase behavior by visual inspection. Phase-boundary lines are indicated clearly in our plots. All simulation images and videos were generated using OVITO[58].

Our approach in this paper is to introduce the idea of a continuum for active matter systems, with limiting cases defined by the activity of the less active (or 'slow') species. When the less active particles are Brownian we have an active/passive mixture. As the activity of the 'slow' species increases we obtain a mixture of two types of particles with distinct activities and velocities (fast and slow). As the activity of the 'slow' species increases further, it approaches the activity of the fast species, until they are equal and then we get a monodisperse active system. Monodisperse active and active/passive systems can be viewed as subsets and limiting cases of this broader active/active continuum. Here, we move between the two extreme cases via two parameters: the fast species' particle fraction (x_f) and the slow species' activity (Pe_s). In our investigation of the active/active phase space we have found two additional quantities. First, the 'net activity' which is an average of each particle's activity weighted by its particle fraction (subscript 's' indicates variables for the slow species and 'f' for the fast species):

$$Pe_{net} \equiv x_s Pe_s + x_f Pe_f. \tag{7}$$

Note that as either of the examined parameters (x_f or Pe_s) is increased the net activity also increases However, Pe_{net} does not account for the relative activity between the two species. To this end we also defined the activity ratio, which is a ratio of the slow particle activity to the fast:

$$Pe_R \equiv \frac{Pe_s}{Pe_f} \tag{8}$$

and varies between zero (for an active/passive mixture) and one (for a monodisperse active system).

3 Background

The onset of MIPS in the ABP model was first examined in monodisperse active systems[6]. In their study, Fily and Marchetti showed that even without symmetry-breaking, active systems will phase separate. They went on to investigate the dynamics of the ABP model and developed a continuum theory constructed from
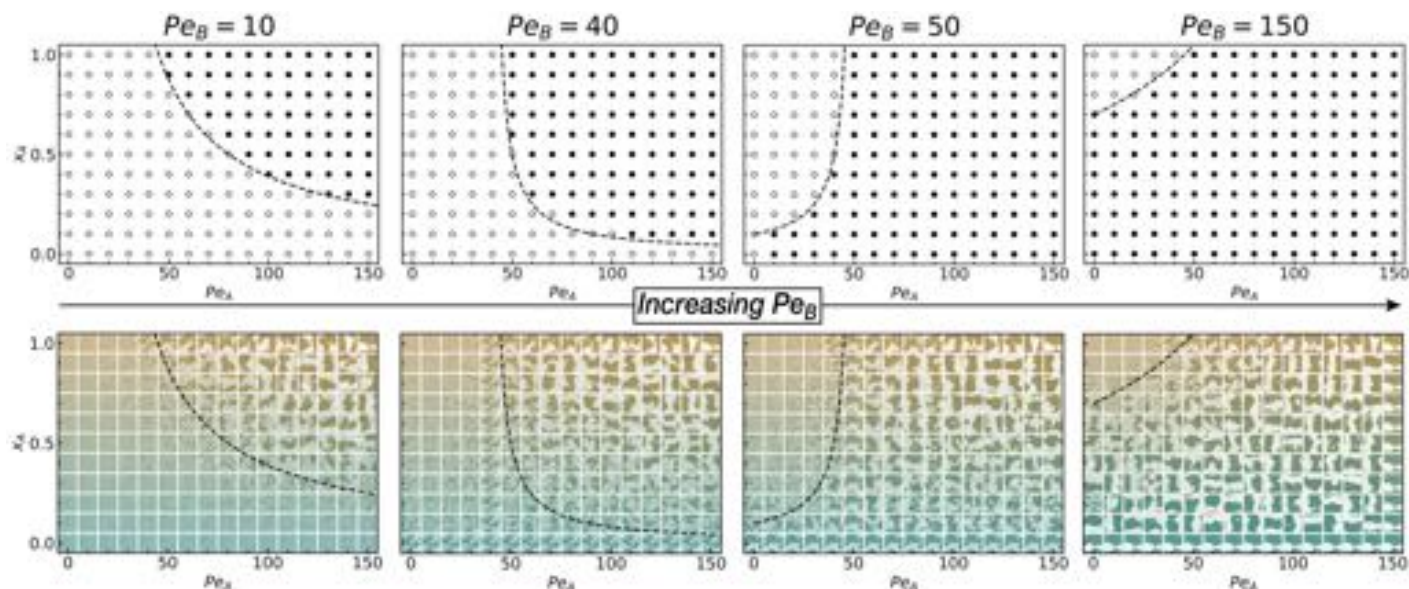
Fig. 2 Top row: Phase diagram in the x_A-Pe_A plane for $Pe_B = 10, 40, 50, 150$. Filled symbols denote phase-separated systems, as determined by our MIPS-identifying algorithm, and open symbols denote a gaseous steady-state. The dashed lines indicate phase boundaries predicted by the active/active equation for ϕ_0 in table 1, which is the theoretical binodal according to our kinetic theory. There is good agreement between the simulations and theory. Bottom row: the same phase diagrams are shown illustrated by simulation (final) snapshots after $300\tau_r$, where 'A' particles are shown in gold and 'B' particles in teal. (See ESI, Fig. S2 for the full parameter range).

an effective, density-dependent, swim-speed. The phase diagram of the ABP model was later investigated by Redner et al.[52] who calculated the densities of the dense and dilute phases versus activity at various area fractions. At all area fractions, increasing activity corresponded to more particles in the dense phase (and, commensurately, fewer particles in the gas phase).

Expanding the phase space, Stenhammar et al. examined binary mixtures of active and passive particles[31]. Aside from the total area fraction and particle activity, an additional parameter was introduced, the particle fraction of each species. It was shown that by increasing either the magnitude of the active species' activity, or the fraction of active particles, the system became more likely to phase separate and MIPS was achieved at lower area fractions of active particles (than in the corresponding monodisperse all-active system). In other words, the presence of passive particles enhanced MIPS. It was also observed that the distribution of particles *within* the dense phase was not homogeneous; instead, there were small domains of predominantly active or predominantly passive particles. The domains were such that the interior of the cluster consisted mostly of trapped passive particles while the edges consisted mostly of active particles. This makes sense considering that for MIPS to persist, the body axis of particles at the cluster edge must form an acute angle with respect to a normal to the cluster surface (or else they simply leave the cluster)[10,52,53]. As a passive particle does not exert an active force it cannot maintain the cluster edge.

Both studies developed a kinetic theory, to predict the conditions necessary for MIPS based upon the parameters of activity and area fraction, thus producing nonequilibrium phase diagrams. In both cases, an assumption was made that there is a steady-state equilibrium between an infinite, hexagonally close-packed, dense phase and a gas phase. Additionally, for an active/passive mixture, the area fraction of active particles in the gas phase (ϕ_g^{act}) and in the dense phase were assumed to be equally proportional to the active particle fraction ($\phi_g x_{act} = \phi_g^{act}$). For a monodisperse active system at steady-state, the derived rates of particle adsorption (from the gas to the dense phase) and desorption (from dense to gas phase) are equal (Table 1). Thus, by writing expressions for these terms and equating them, Redner et al. obtained a theoretical description for the density of each phase[52].

	Monodisperse Active	Binary Active/passive	Binary Active/active
	(Redner et al.[52])	(Stenhammar et al.[31])	(this study)
k_{in}	$\dfrac{4\phi_g v_0}{\pi^2 \sigma^2}$	$\dfrac{4\phi_g^{act} v_0}{\pi^2 \sigma^2}$	$\dfrac{4(\phi_g^s v_0^s + \phi_g^f v_0^f)}{\pi^2 \sigma^2}$
k_{out}	$\dfrac{\kappa D_r}{\sigma}$	$\dfrac{\kappa D_r}{\sigma}$	$\dfrac{\kappa D_r}{\sigma}$
ϕ_0	$\dfrac{3\pi^2 \kappa}{4Pe}$	$\dfrac{3\pi^2 \kappa}{4x_{act}Pe}$	$\dfrac{3\pi^2 \kappa}{4(x_s Pe_s + (1-x_s)Pe_f)}$

Table 1 Expressions for rates of adsorption on to (k_{in}) and desorption from (k_{out}) the dense phase as well as the area fraction at which MIPS is first observed (ϕ_0), for: monodisperse active, active/passive, and active/active systems. The more complex active/passive and active/active expressions reduce to the simpler monodisperse case.

In introducing a second (passive) species, these rates remain equal, but the new expression included the effect of the particle fraction of each species[31]. For both studies, particle desorption was assumed to occur in cascading, 'avalanche' events, resulting in a fitting parameter κ. It is important to note that this approach

assumes the existence of a hexagonally close-packed dense phase, and as such, it is not a good approximation at very high or very low area fractions.

4 Results

4.1 Kinetic theory & phase diagram

By removing the restriction that the slow particles be passive, we introduced another parameter, the activity of the second species. To populate this new phase diagram we restricted our study to total area fraction $\phi = 0.6$ to ensure that we were examining a sufficiently high total area fraction to observe monodisperse MIPS ($\phi > 0.45$). We simulated $N = 15,000$ particles and systematically varied three parameters: the activity of each species A, B, ($Pe_{A,B} = [0,150]$) and the particle fraction ($x_A = [0.0, 1.0]; x_B = 1 - x_A$), resulting in 1,232 simulations in total (fig. 2). Figure 2 shows four representative slices of the three dimensional phase diagram for this space, where Pe_B was held constant at 10, 40, 60 and 150. Each x_A-Pe_A plane is a phase diagram showing whether MIPS occurred, as computed by our MIPS algorithm and denoted by filled points. In the bottom row of figure 2, the same phase diagrams are shown illustrated by simulation (final) snapshots after $300\tau_r$. On any given plane, increasing the fraction of the more active species (moving up along a column if $Pe_A > Pe_B$ or down a column if $Pe_A < Pe_B$), or increasing the activity of species A (to the right on a given row) gives parameters more conducive to MIPS. Similarly, as we increased the activity of species B (fig. 2, left to right), more of the phase plane becomes phase separated. To distill these data, we found that the propensity for a system to undergo MIPS increased as the activity of any constituent species increased or as the fraction of the more active species increased (fig. 2). It is important to note that the computational timescale used in the studies comprising figure 2 ($\tau_r = 300$) is likely not sufficient to observe the nucleation and growth of some metastable states, namely those which are proximal to the binodal[59]. Only by simulating on much longer timescales or by computationally seeding cluster nucleation can we access the long-time behavior of such metastable systems.

We also extended the existing kinetic theories of monodisperse active[52] and passive/active[31] systems, summarized in section 3 to include a second active species. In examining the rate of adsorption (k_{in}) and desorption (k_{out}), we continued to make the assumption of previous models that desorption from the dense phase to the gas is governed exclusively by rotational diffusion (and is therefore identical for each particle, given they are the same size and equilibrated in the same heat bath). However, adsorption from the gas onto the dense phase depends on particle activity, because the more active particles have a larger persistence length (l_p) and therefore collide with the dense phase more readily. Our expressions for k_{in} and k_{out} for active/active systems are presented in table 1; where ϕ_g is the density of a given species in the gas phase (subscript g)[52].

We then considered dimensionless variables and extended what has been reported as a 'binodal relation' ($\phi_g^{act} = x_{act}\phi_0$) developed by Stenhammar et al.[31] for passive/active systems to now include a second active species, which gives the binodal conditions:

$\phi_g^A = x_A\phi_0$ and likewise $\phi_g^B = (1-x_A)\phi_0$ for active species A and B. The two together can be summarized by the sole relation initially developed by Redner et al.[52], $\phi_0 = \phi_g^A + \phi_g^B = \phi_g$. The relation produced by equating the flux at the cluster edge does, in fact, predict very reliably, the onset of MIPS in simulation. However, we should note that this is not a binodal in the strict thermodynamic sense, namely there is no equilibration of a thermodynamic quantity between phases. Substituting these relations into the expressions for k_{in} in Table 1, we can obtain an expression that relates activity, particle fraction and area fraction to phase separation (table 1, ϕ_0 in column active/active), where, if $\phi_0 \leq \phi$ the system will undergo MIPS. This theoretical 'binodal' should ideally separate closed (phase separated) points from open points, as identified from our simulation data. Our extension of this kinetic theory demonstrates strong agreement with simulation as seen in figure 2, where, the theory is represented by the dashed line on each plane. We used $\kappa = 3.65$, which produced the best fit across the phase space examined in this study. While this kinetic theory outlines the binodal of the first-order MIPS phase transition, we do not investigate the potential for additional complex phenomena within the dense phase (e.g. hexatic phase[52], grain boundary motion, or dislocation glide). The study of such phenomena via principal component analysis or machine learning is an important future direction for binary active/active mixtures.

4.2 Phase behavior

In figure 3 we show characteristic snapshots of the system at different slow particle activity and particle fraction. As the systems are highly dynamic, we suggest the reader watch the videos for each snapshot as well (ESI)†. The snapshots qualitatively show how the emergent phenomena characteristic of active/passive mixtures transitions to the distinct steady-state behavior of monodisperse active systems. The columns in figure 3 correspond to four different slow activities that are representative of this phase space: $Pe_s = 0$ (Brownian), 25 ($< Pe_{MIPS}$ below the activity required for MIPS if the system were monodisperse), 100 ($> Pe_{MIPS}$ above the activity sufficient for MIPS if the system were monodisperse), and 200 (about half of the fast species activity). Rows correspond to three particle fractions, $x_f = 0.3, 0.5$, and 0.7 in order to examine majority slow, equal, and majority fast mixtures respectively.

In the case of an active/passive mixture (fig. 3, left column (a),(e),(i)) we found agreement with previous studies[31], (see also section 3), both in terms of structure and dynamics, an additional verification of our velocity-variant model. We now discuss the effect of changing the particle fraction for an active/passive system. For a system composed entirely of passive particles ($x_f = 0$), MIPS did not occur and the system remained a homogeneous gas undergoing random Brownian diffusion. If we substitute a small fraction of passive particles for active particles (e.g. $x_f = 0.05$) the resulting system still remained in the gaseous state. The small number of fast active intruders left temporary wakes behind them as they swam through the majority passive gas (ESI, movie and fig. S4)†, as has been observed in the literature[60]. Increasing the fraction of fast particles further
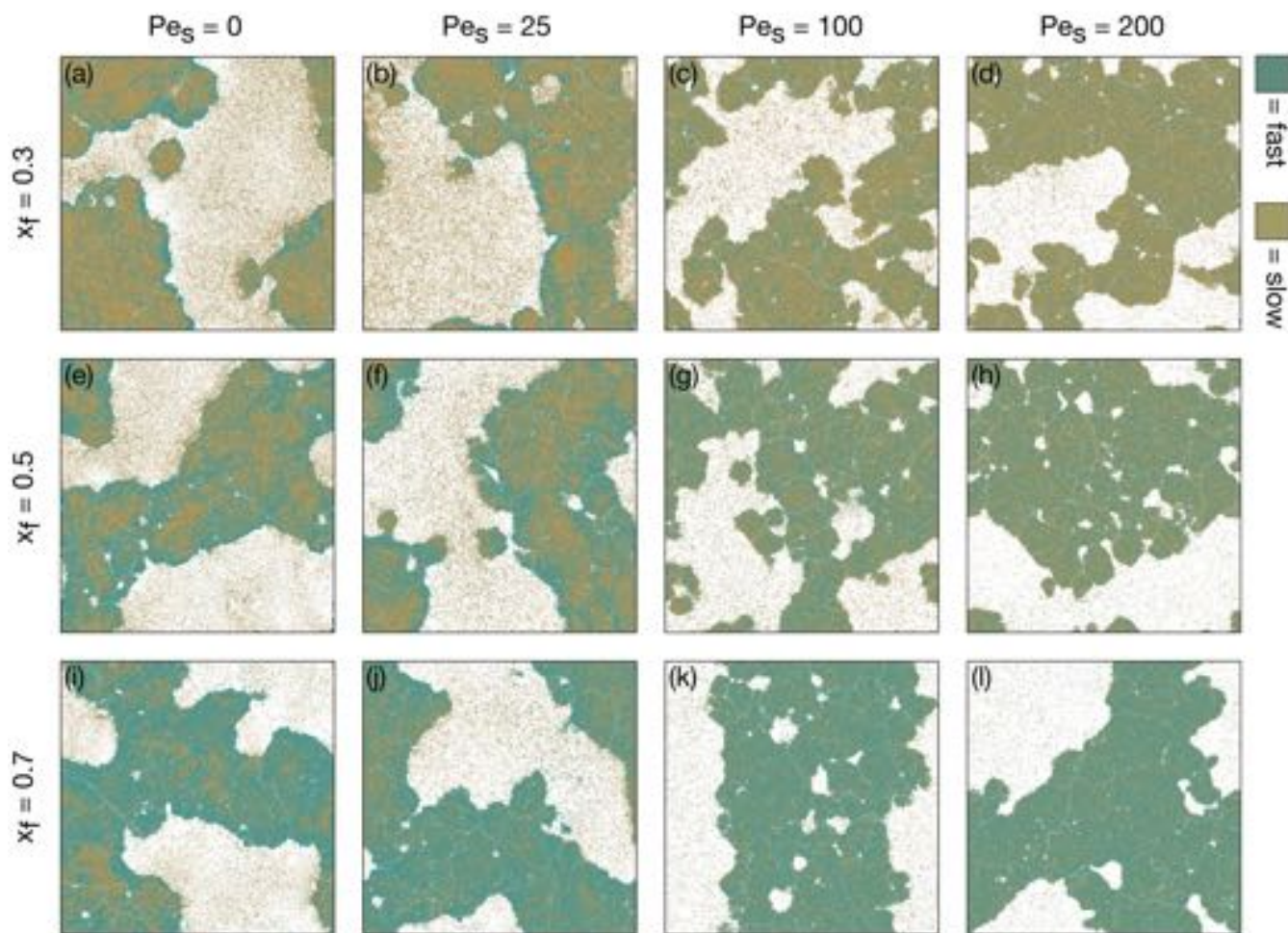
Fig. 3 (Video online) Simulations of active Brownian particles with distinct slow (gold) and fast ($Pe_f = 500$, teal) particle fractions and activities. All snapshots were taken after steady-state had been reached, $\tau_r = 300$. The particle fraction is constant in each row: $x_f = 0.3$, 0.5, and 0.7; illustrating majority slow, equal and majority fast mixtures respectively. The activity of the slow species is constant in each column: $Pe_s = 0$, 25, 100, and 200. The activity of the fast species is fixed at $Pe_f = 500$.

($x_f = 0.1$), small clusters formed and were quickly annihilated as a thin outer edge of fast particles pushed through the passive interior (ESI, movie and fig. S5)†. At the particle fraction necessary for MIPS ($x_f = 0.15$); there was still a majority of passive species and a small number of very fast active particles. This was perhaps the most volatile system to undergo sustained MIPS in that clusters engaged in fission and fusion events repeatedly, yet, the dense phase was never absent entirely and the system still coarsened in time. Fast particles predominated at the cluster edge and pushed the slower particles into the dense phase (similar to fig. 3(a)). The clusters here seemed to be qualitatively different to the clusters that occur through MIPS in typical monodisperse active systems[52] due to their volatility. Increasing the fraction of fast particles further ($x_f > 0.15$) did not prevent partial segregation by particle type, but, the system behavior gradually moved toward a monodisperse (fast) active system becoming markedly less volatile as fast particle fraction increased (fig. 3(e), (i)).

   By turning on the activity of the slow species (fig. 3, (b)), we observed how an active slow component altered the system behavior. Note that a monodisperse system prepared at $Pe_s = 25$

with the same total system density is below the required activity for MIPS. We found the same trends with respect to particle fraction as in the active/passive case. Below the fast particle fraction required for phase separation (now $x_f^{MIPS} = 0.05$), we found a gas with few active tracers where the path left by the fast component now collapsed more quickly (as the slow component did not rely on Brownian diffusion to consume the void left by the fast particle). As fast particle fraction increased (fig.3 (f), (j)), we obtained the same behaviors present in the active/passive case with a seeming decrease in system volatility. The partial segregation by particle type observed in active/passive systems, persisted when the slow species was active, but to a lesser extent. Ultimately, there was no discontinuous jump in system behavior with respect to slow activity and particle fraction.

   As we continued increasing the slow activity (e.g. for $Pe_s = 100$, 200, see fig. 3 (c),(d)), the system underwent MIPS regardless of fast particle fraction. Additionally, the distribution of each particle type appeared homogeneous, with no prevalent species at the cluster edge nor in domains in the cluster interior. For systems prepared at a slow activity that was sufficiently high for MIPS,

we found that the particle fraction controlled the participation of particles in the dense phase between the limiting cases of a monodisperse slow system (for $x_f \to 0$) and a monodisperse fast system (for $x_f \to 1$). As the slow particle activity approached that of the fast species, system volatility decreased.

As one of the characteristics of a mixture is the distribution of particles in each phase, with the most extreme case being a partially segregated dense phase of an active/passive mixture, we can qualitatively distinguish two regimes. One where phase separation also shows segregation by type (active/passive is included here) and a second regime where there is a more homogeneous dense phase (even though $Pe_s \neq Pe_f$). In other words, keeping the fast activity constant, at low slow activity the system behaves like an active/passive mixture and at high slow activity the system behaves like a monodisperse active system.

4.3 Steady state composition of dense phase

To gain more insight and obtain a quantitative understanding of the two regimes observed, we computed the dense-phase composition after steady-state had been reached. To examine the effect of mixing, we compared the composition of the equivalent monodisperse system for each simulation, *i.e.* one with the same total area fraction and activity. For example, in figure 4a, diamond teal symbols show the percentage of fast particles in the dense phase as a function of the fast particle fraction, at constant slow activity $Pe_s = 50$ and constant fast activity $Pe_f = 500$. The teal dashed line at $\approx 98\%$ shows the percentage of fast particles in the dense phase for a monodisperse active system of fast particles at $Pe = 500$. Similarly, for slow particles, gold triangles show the percentage of slow particles in the dense phase as a function of the fast particle fraction, for constant slow activity $Pe_s = 50$ and constant fast activity $Pe_f = 500$. The brown dashed line at $\approx 45\%$ shows the percentage of slow particles in the dense phase for a monodisperse active system of slow particles with $Pe = 50$.

In regime I ($Pe_s \lesssim 110$), we observed deviations in the steady-state composition of each species in the dense phase with respect to a monodisperse system (of the same activity, fig. 4a). We found that the faster species experienced a suppression in the percentage of particles participating in the dense phase relative to its monodisperse counterpart. The slower species experienced the opposite effect, the steady-state participation in the dense phase was enhanced upon being mixed with a faster species.

In regime II ($Pe_s \gtrsim 110$), the enhancement and suppression characteristic of regime I have disappeared (i.e. are within error of a monodisperse system of either type). Instead, each species, regardless of what it was being mixed with, assumed the same percentage of particles participating in the dense phase as a monodisperse system of the same activity (fig. 4b). This result is counterintuitive: as fast and slow activities approach one another but while still very different (e.g. $Pe_s = 200$ and $Pe_f = 500$ fig. 4b), each species behaved as if it weren't mixed at all, as long as Pe_s was sufficiently high. The significance of the slow particle activity at which this regime change occurs, as well as its dependence on parameters not studied here (*e.g.* the total area fraction) are of great interest to the authors and require further study.

Our data gives a clear relationship for which parameters affect the magnitude of the enhancement or suppression effect that is found in regime I. The trends in these data are most evident in figure 4c, where we show percent difference between the dense phase of a mixture and a monodisperse system, versus the slow particle activity. The fast species is always suppressed (relative to a monodisperse fast system, bottom half of fig. 4c) just as a slow species can only be enhanced (relative to a monodisperse slow system, top half of fig. 4c). We see that for any set slow activity, the extent of the enhancement and/or suppression was dependent on both the particle fraction and activity ratio. Moreover, the particle fraction was found to control the dominant behavior (suppression/enhancement) for a given system. A system composed of a majority of fast particles predominantly undergoes enhancement of the slow species (fig. 4a, $x_f = 0.9$) just as a majority slow system primarily exhibits suppression (fig. 4a, $x_f = 0.1$). The activity ratio was found to control the amount of suppression/enhancement. For low activity ratio, both enhancement and suppression are amplified (fig. 4a, $Pe_R = 0.1$) and for activity ratio close to unity the effect is greatly reduced (and evidently nonexistent at $Pe_R = 1$). Additionally, both behaviors need not occur in a given system at the same time (*e.g.* in fig. 4a, at $x_f \geq 0.5$ the slow species is being enhanced while the fast species is not being that suppressed).

To contextualize this result we relate to active/passive systems. In active/passive systems the slow (passive) species is being 'pushed' into the dense phase by the fast species (enhanced relative to a monodisperse passive system which does not undergo MIPS at all). We have shown that this finding is not exclusive to an active/passive mixture, in fact, this effect can be found at slow particle activity far above the activity required for MIPS in a monodisperse system ($Pe_{MIPS} \approx 45$ for $\phi = 0.6$). The extent of the enhancement/suppression decays asymptotically with respect to the slow activity. As such, our 'regime II' simply indicates that the asymptotic decay has approached close enough to zero so that the effect of enhancement or suppression is within standard deviation of the steady-state cluster participation.

4.4 Dynamic behavior

We then examined the formation and growth of the dense phase on short timescales. We found that both fast and slow species nucleated the dense phase at the same time, however, the rate of growth of each species was distinct where the more active component would add to the dense phase more rapidly (ESI, fig. S6)†. Additionally, we report that the early-stage dense phase composition did not track that of a monodisperse system of either the slow or fast particle type. This effect is observed upon varying activity ratio at constant particle fraction and upon varying particle fraction at constant activity ratio (given that x_f and $Pe_R \neq 0, 1$). At constant particle fraction (fig. 5a), increasing the activity ratio corresponds to a faster rate of decomposition into the dense phase (increasing Pe_R brings lines closer to a monodisperse system of fast particles, maroon dashed line). The same behavior was observed at constant activity ratio (fig. 5b) for increasing fast particle fraction (dark purple dashed line).
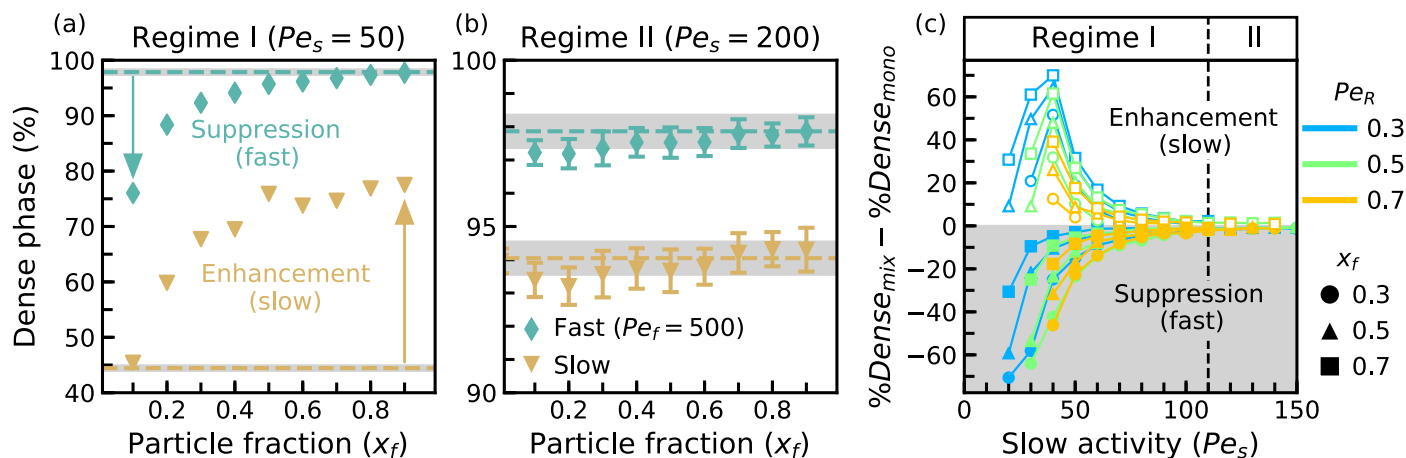
Fig. 4 Steady-state participation in the dense phase for both fast and slow species. (a, b) Percentage of each particle type in the dense phase for different particle fraction in (a) regime I ($Pe_s = 50$) and (b) regime II ($Pe_s = 200$) compared to a monodisperse system of each particle type (dashed lines). Error bars are shown when larger than the symbol size and in grey shading for monodisperse systems. (a) In regime I slow species experience enhancement and fast species exhibit suppression with respect to a monodisperse system of the same total area fraction. (b) In regime II fast and slow species assume the dense phase participation (within error) of a monodisperse fast or slow system respectively. These data are condensed in (c) a plot of the difference in the percent participation in the dense phase between a mixed and monodisperse system at distinct activity ratios and particle fractions. Negative values (filled symbols) indicate suppression of the fast component and positive values (unfilled symbols) show enhancement of the slow component. Regime I persists for systems that undergo MIPS with slow activity up to $Pe_s \approx 110$ and activity ratio less than unity. Beyond this point, each species assumes the steady-state participation in the dense phase correspondent to a monodisperse simulation at the same activity and total system area fraction.

Both of these observations can be captured by the net activity, whereby increasing the net activity, a system either moves a homogeneous gas closer to the binodal line or causes a greater percentage of particles to join the dense phase, at a quicker rate. While in sections 4.2 and 4.3 we showed that active/active mixtures at steady state take on the characteristics of an active/passive mixture or monodisperse active system, the dynamic behavior of binary active systems is distinct from either extreme case.

As demonstrated in figure 5c, the net activity also affects the nucleation time of an active system. We extracted the time that the mean cluster size began to increase (fig. 5c, inset) and plotted this against the net activity on a log-log scale (fig. 5c). The initial nucleation event has a power law dependence on the net activity with exponent $-6/5$, (fig. 5c), where a higher net activity corresponds to a faster nucleation time. This phenomenon is also dependent on the activity ratio, as such, we fit data at constant activity ratio to a fixed power law and renormalize the nucleation time by the produced constant (e^b, where b is a function of the activity ratio). However, this renormalization (and thus the activity ratio) does not affect the exponent of the power law. So, the net activity (an intrinsic quantity) sets a single time for cluster nucleation, independent of the activity of individual species. Growth of the cluster thereafter is controlled by each species' activity, where an increase in the net activity corresponds to more rapid coarsening rate.

4.5 Net activity

So far, we have observed the importance of the net activity in a number of ways: setting the repulsive potential, as a component of our kinetic theory, and being a key quantity in describing

the trends of active/active mixtures (*e.g.* a high net activity corresponds to faster nucleation times). We now show the further utility of the net activity, specifically, how it dictates MIPS into dense and dilute phases of varying area fractions.

We found that, similar to activity in monodisperse systems, the net activity outlines the binodal of coexisting area fractions at steady state (fig. 6a). At low net activity ($Pe_{net} < 45$), we observed that the majority of particles participated in the gas phase at steady state. As the net activity increased ($Pe_{net} \geq 45$), we found that the area fraction of the dense phase exceeded that of the gas phase. The surplus of particles participating in the dense phase grew more drastic as the net activity continued to increase. To further quantify this transition we introduced an order parameter, the difference in the area fraction of dense and dilute phases (normalized by the total system area fraction),

$$m = \frac{\phi_l - \phi_g}{\phi}. \tag{9}$$

Many studies have attempted to determine the universality class of the MIPS phase transition and have reported the critical area fraction for monodisperse MIPS ($\phi_c = 0.6$, the same value used in this study). As our expression for the net activity reduces to the activity for a monodisperse system (for $x_f \to 0, 1$ or $Pe_s = Pe_f$), we examined the critical point of this first-order phase transition with respect to the net activity. Similar to Siebert et al.[47], we examined the inverse net activity in place of temperature. We extracted the critical inverse net activity, that is the inverse net activity when the order parameter is zero, $Pe_{net,c}^{-1} \approx 1/45$, (fig. 6b). While the data proximal to the zero-crossing of the order parameter is admittedly sparse in this study, we found fair agreement with the critical activity reported in similar studies
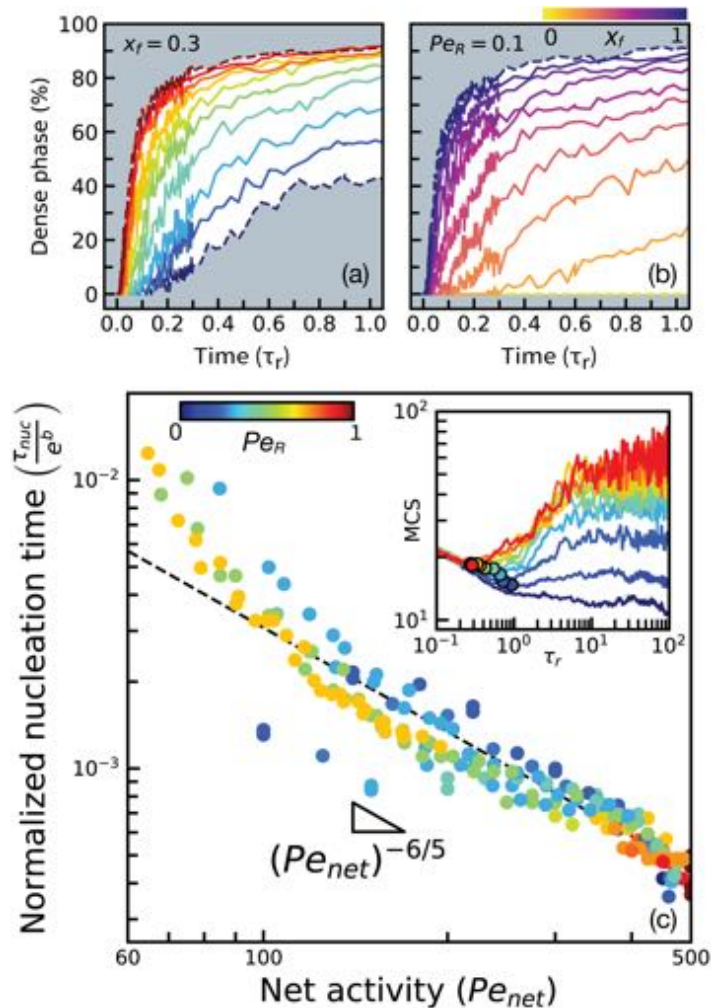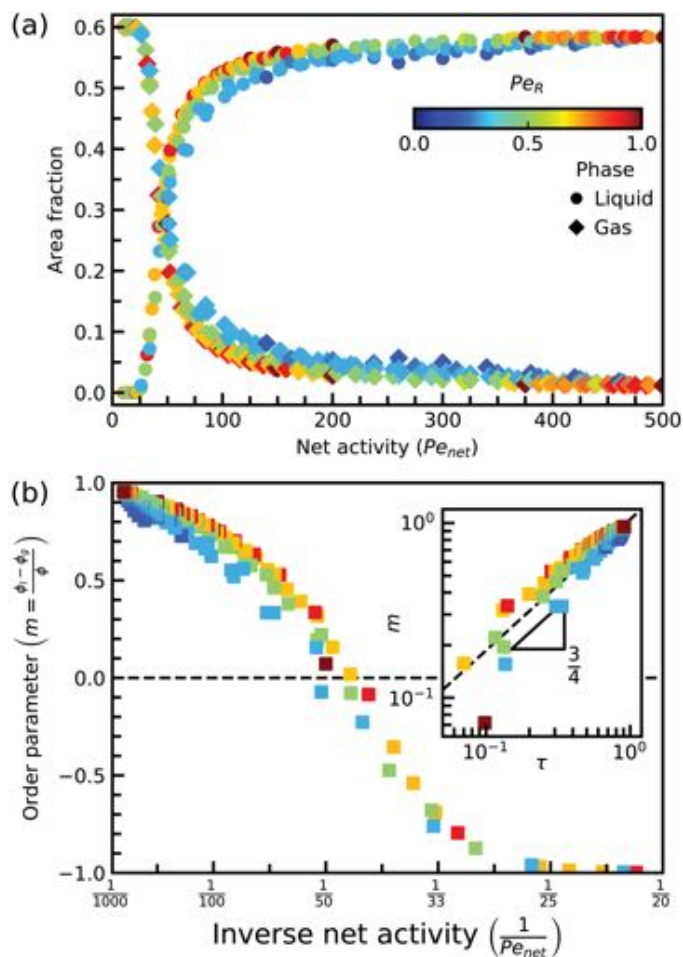
Fig. 5 Time-resolved participation of all particles in the dense phase at constant particle fraction ($x_f = 0.3$) showing the effect of changing slow particle activity is shown in (a). Colorbar indicates the activity ratio of each simulation ($Pe_f = 500$). Constant activity ratio (b, $Pe_R = 0.1$) illustrates the effect of varying the particle fraction (where shade indicates each simulated particle fraction and dashed lines indicate monodisperse systems). Dynamic data shows a power-law relationship between nucleation time and net activity (c). Nucleation time is normalized by a constant (e^b) for each value of the activity ratio to emphasize the common slope of the data. Points are collapsed from a wide variety of activity ratios (Pe_R), particle fractions (x_f), and fast particle activities (Pe_f). Inset shows computation of the nucleation time, taken as the local minimum in the mean cluster size vs. time.

Fig. 6 Steady-state area fraction of liquid (circles) and gas (diamonds) states outline a binodal when plotted against net activity (a). Activity ratio (color), appears to account for minor deviations from complete collapse of the data. Order parameter of systems at steady-state (b) where increasing the inverse net activity corresponds to a transition to the gas phase. Zero-crossing of the order parameter (dashed line) gives the inverse net activity at the critical point ($Pe_{net,c}^{-1} = 1/45$). (Inset) Determination of the critical exponent β with respect to the reduced inverse net activity ($m = (-\tau)^\beta$) gives $\beta = 3/4$ (with residual $r^2 = 0.96$ for linear scales).

of monodisperse systems (Pe_c 45 in this study as compared to $Pe_c = 40$)in ref.[47]. We then constructed the reduced inverse net activity,

$$\tau = \frac{Pe_{net}^{-1} - Pe_{net,c}^{-1}}{Pe_{net,c}^{-1}}. \quad (10)$$

Extracting the slope from a plot of the order parameter versus the reduced inverse net activity, we determined the critical exponent $\beta = 3/4$, for $m = (-\tau)^\beta$, (fig. 6b inset). This value is distinct from previously reported values; both for simulation-based studies ($\beta = 1/2$)[47], and in theoretical examinations ($\beta = 1/8$ in agreement with the 2D-Ising model)[61]. To further probe the va-

lidity of the exponent reported in this study, more simulation data proximal to the inverse critical net activity is required.

5 Conclusion

We computationally studied mixtures of active particles of different activities and thus velocities (fast and slow). We calculated the binodal envelope for MIPS in the particle fraction-activity phase space and extended existing kinetic theories on monodisperse active and active/passive systems to incorporate a second active species. Our extended kinetic theory was in good agreement with simulations for the binary systems studied here.

In analyzing the dynamics and steady-state behaviors of active/active systems we summarize the main findings and discuss implications. Emergent phenomena known from monodisperse active matter and from active/passive mixtures (*e.g.* MIPS, segregation by particle type, volatility *etc.*) can be tuned to appear or vanish in active/active mixtures showing that these phenomena

are part of a continuum of behaviors. We can however categorize into two mixing regimes: (i)Regime I: the faster/slower particles experience suppressed/enhanced participation in the dense phase due to mixing. (ii) Regime II: each particle type participates in the dense phase as if it were a monodisperse system. The two regimes and the transition between them indicates that there is a tolerance of the emergent behaviors with respect to the two species' activities, i.e. there is a whole range of parameters for which we see each regime. It is interesting to note, for example, that the transition between the two regimes for the systems studied here occurs when $Pe_s \approx 110$ regardless of the fast activity (for activity ratio $Pe_R = 0.1 - 0.9$ in steps of 0.1). In other words, the two activities in a mixture can be quite different in magnitude and still the system would act like a monodisperse active system. This could explain the robustness of natural swarms where we might expect that differences in the velocities of animals/organisms would not immediately result in a collapse of the group (swarm) behavior. Moreover, this transition between a regime where there is segregation by type due to distinct activities and a regime where the system acts like a monodisperse homogeneous one could have implications in biological systems such as liquid-liquid phase separation in the cell[62]. For example, it could be that distinct activities contribute (together with other interactions) to phase separation and a change in the activities of two species could regulate transitioning from a gas (no MIPS) to a phase separated state with segregated domains (regime I) to a mixed dense phase (regime II). Furthermore, one quantity naturally emerges from our analysis, capturing the physics of these mixtures: the net activity (eq. 7). The net activity gives the repulsive strength and is a natural result of a simple kinetic theory for this system. It provides a clearly defined binodal and coincides with previously studied limiting cases of active/active mixtures, (monodisperse active and active/passive systems).

While our results demonstrate the complex behavior that is accessible to multi-component active mixtures, the work presented here is only the first step. A number of interesting future directions emerge. We expect that a greater degree of control is achievable in synthetic active matter via the introduction of additional active species (as is the case in biological contexts). Furthermore, a mixture of active species (distinct in their activity) gives an intriguing setup for the examination of potential thermodynamic quantities that set the characteristics of active matter, such as the active pressure and its implications regarding an equation of state[20,63–65].

Acknowledgments

References

1 R. Di Leonardo, L. Angelani, D. Dell'arciprete, G. Ruocco, V. Iebba, S. Schippa, M. P. Conte, F. Mecarini, F. De Angelis and E. Di Fabrizio, PNAS, 2010, **107**, 9541–5.

2 T. Vicsek, A. Czirók, E. Ben-Jacob, I. Cohen and O. Shochet, Physical Review Letters, 1995, **75**, 1226–1229.

3 H. C. BERG and D. A. BROWN, Nature, 1972, **239**, 500–504.

4 M. J. Schnitzer, Physical Review E, 1993, **48**, 2553–2568.

5 M. E. Cates and J. Tailleur, Annual Review of Condensed Matter Physics, 2015, **6**, 219–244.

6 Y. Fily and M. C. Marchetti, Physical Review Letters, 2012, **108**, year.

7 A. P. Solon, H. Chaté and J. Tailleur, Physical Review Letters, 2015, **114**, 068101.

8 R. W. Nash, R. Adhikari, J. Tailleur and M. E. Cates, Physical Review Letters, 2010, **104**, 258101.

9 J. Bialké, J. T. Siebert, H. Löwen and T. Speck, Physical Review Letters, 2015, **115**, year.

10 A. Patch, D. M. Sussman, D. Yllanes and M. C. Marchetti, Soft Matter, 2018, **14**, 7435–7445.

11 D. Loi, S. Mossa and L. F. Cugliandolo, Physical Review E - Statistical, Nonlinear, and Soft Matter Physics, 2008, **77**, year.

12 S. C. Takatori and J. F. Brady, Soft Matter, 2015, **11**, 7920–7931.

13 M. E. Cates and J. Tailleur, EPL, 2013, **101**, year.

14 J. Tailleur and M. E. Cates, Physical Review Letters, 2008, **100**, year.

15 S. C. Takatori and J. F. Brady, Physical Review E - Statistical, Nonlinear, and Soft Matter Physics, 2015, **91**, year.

16 M. Rein and T. Speck, The European Physical Journal E, 2016, **39**, 84.

17 T. F. F. Farage, P. Krinninger and J. M. Brader, Physical Review E, 2015, **91**, 042310.

18 U. M. B. Marconi, N. Gnan, M. Paoluzzi, C. Maggi and R. Di Leonardo, Scientific Reports, 2016, **6**, 23297.

19 Y. Fily, A. Baskaran and M. F. Hagan, The European Physical Journal E, 2017, **40**, 61.

20 A. P. Solon, J. Stenhammar, R. Wittkowski, M. Kardar, Y. Kafri, M. E. Cates and J. Tailleur, Physical Review Letters, 2015, **114**, 198301.

21 A. P. Solon, J. Stenhammar, M. E. Cates, Y. Kafri and J. Tailleur, New Journal of Physics, 2018, **20**, year.

22 I. Buttinoni, J. Bialké, F. Kümmel, H. Löwen, C. Bechinger and T. Speck, Physical Review Letters, 2013, **110**, year.

23 M. Driscoll and B. Delmotte, Current Opinion in Colloid & Interface Science, 2019, **40**, 42–57.

24 X. Yang, M. L. Manning and M. C. Marchetti, Soft Matter, 2014, **10**, 6477–6484.

25 S. Das, G. Gompper and R. G. Winkler, New Journal of Physics, 2018, **20**, 015001.

26 P. S. Mahapatra, A. Kulkarni, S. Mathew, M. V. Panchagnula and S. Vedantam, Physical Review E, 2017, **95**, 062610.

27 C. Kurzthaler, S. Leitmann and T. Franosch, Scientific Reports, 2016, **6**, 36702.

28 M. Pu, H. Jiang and Z. Hou, Soft Matter, 2017, **13**, 4112–4121.

29 Y. Fily, S. Henkes and M. C. Marchetti, Soft Matter, 2014, **10**, 2132–2140.

30 P. Dolai, A. Simha and S. Mishra, Soft Matter, 2018, **14**, 6137–6145.

31 J. Stenhammar, R. Wittkowski, D. Marenduzzo and M. E. Cates, Physical Review Letters, 2015, **114**, 018301.

32 R. Wittkowski, J. Stenhammar and M. E. Cates, New Journal of Physics, 2017, **19**, 105003.

33 S. Ramananarivo, E. Ducrot and J. Palacci, Nature Communications, 2019, **10**, 3380.

34 A. K. Omar, Y. Wu, Z.-G. Wang and J. F. Brady, ACS Nano, 2019, **13**, 560–572.

35 G. Pessot, H. Löwen and A. M. Menzel, arXiv:1907.13583, 2019, 3401–3408.

36 M. Theves, J. Taktikos, V. Zaburdaev, H. Stark and C. Beta, Biophysical Journal, 2013, **105**, 1915–1924.

37 E. Ben-Jacob, A. Finkelshtein, G. Ariel and C. Ingham, Trends in Microbiology, 2016, **24**, 257–269.

38 A. J. King, A. M. Wilson, S. D. Wilshin, J. Lowe, H. Haddadi, S. Hailes and A. J. Morton, Selfish-herd behaviour of sheep under threat, 2012.

39 B. Pettit, Z. Ákos, T. Vicsek and D. Biro, Current Biology, 2015, **25**, 3132–3137.

40 N. H. Nguyen, D. Klotsa, M. Engel and S. C. Glotzer, Physical Review Letters, 2014, **112**, 075701.

41 K. Yeo, E. Lushi and P. M. Vlahovska, Soft Matter, 2016, **12**, 5645–5652.

42 R. Wittmann, J. M. Brader, A. Sharma and U. M. B. Marconi, Physical Review E, 2018, **97**, 012601.

43 S. N. Weber, C. A. Weber and E. Frey, Phys. Rev. Lett., 2016, **116**, 058301.

44 J. Smrek and K. Kremer, Physical Review Letters, 2017, **118**, 098002.

45 A. Y. Grosberg and J.-F. Joanny, Phys. Rev. E, 2015, **92**, 032118.

46 I. Ahmed, D. Q. Ly and W. Ahmed, Materials Today: Proceedings, 2017, **4**, 65–74.

47 J. T. Siebert, F. Dittrich, F. Schmid, K. Binder, T. Speck and P. Virnau, Physical Review E, 2018, **98**, year.

48 S. Thutupalli, D. Geyer, R. Singh, R. Adhikari and H. A. Stone, Proceedings of the National Academy of Sciences of the United States of America, 2018, **115**, 5403–5408.

49 B. Hancock and A. Baskaran, Physical Review E - Statistical, Nonlinear, and Soft Matter Physics, 2015, **92**, year.

50 B. Liebchen and H. Löwen, Accounts of Chemical Research, 2018, **51**, 2982–2990.

51 J. Stenhammar, D. Marenduzzo, R. J. Allen and M. E. Cates, Soft Matter, 2014, **10**, 1489–1499.

52 G. S. Redner, M. F. Hagan and A. Baskaran, Physical Review Letters, 2013, **110**, year.

53 G. S. Redner, A. Baskaran and M. F. Hagan, Physical Review E, 2013, **88**, 012305.

54 J. A. Anderson, C. D. Lorenz and A. Travesset, Journal of Computational Physics, 2008, **227**, 5342–5359.

55 J. Glaser, T. D. Nguyen, J. A. Anderson, P. Lui, F. Spiga, J. A. Millan, D. C. Morse and S. C. Glotzer, Computer Physics Communications, 2015, **192**, 97–107.

56 T. Speck, A. M. Menzel, J. Bialké and H. Löwen, Journal of Chemical Physics, 2015, **142**, year.

57 E. S. Harper, M. Spellings, J. Anderson and S. C. Glotzer, Zenodo, 2016.

58 A. Stukowski, Modelling and Simulation in Materials Science and Engineering, 2010, **18**, 015012.

59 D. Richard, H. Löwen and T. Speck, Soft Matter, 2016, **12**, 5257–5264.

60 C. Reichhardt and C. J. Reichhardt, Physical Review E - Statistical, Nonlinear, and Soft Matter Physics, 2015, **91**, year.

61 B. Partridge and C. F. Lee, Physical Review Letters, 2019, **123**, year.

62 A. A. Hyman, C. A. Weber and F. Jülicher, Annual Review of Cell and Developmental Biology, 2014, **30**, 39–58.

63 S. C. Takatori and J. F. Brady, Current Opinion in Colloid & Interface Science, 2016, **21**, 24–33.

64 Y. Fily, Y. Kafri, A. P. Solon, J. Tailleur and A. Turner, Journal of Physics A: Mathematical and Theoretical, 2018, **51**, 044003.

65 A. P. Solon, Y. Fily, A. Baskaran, M. E. Cates, Y. Kafri, M. Kardar and J. Tailleur, Nature Physics, 2015, **11**, 673–678.

Continuum of active systems

binary mixtures
active/passive

binary mixtures
active/active

monodisperse
active